Version: Post-print

Closed-Form Model and Parametric Study on Connection of Concrete-Filled FRP Tubes into Concrete Footings by Direct Embedment

Pedram Sadeghian, M.ASCE [1] and Amir Fam, M.ASCE [2]

ABSTRACT

Concrete-filled fiber reinforced polymer (FRP) tubes (CFFTs) have been introduced as a new system for piles, columns and poles. A simple moment connection based on direct embedment of the CFFT into concrete footings or pile caps, without using dowel bar reinforcement, has been proposed by the authors. Robust analytical models to predict the critical embedment length (X_{cr}) were also developed and experimentally validated. In this paper, a comprehensive parametric study is carried out using the models developed earlier along with a newly developed closed-form model for the general case of axial loading, bending and shear, applied to the CFFT member. The parameters studied are the diameter (D), thickness (t), length outside the footing (L), and laminate structure of the FRP tube, as well as the tube-concrete interface bond strength (τ_{max}), concrete compressive strength in the CFFT ($f_{ct}{}'$) and footing ($f_c{}'$), and the magnitude and eccentricity of axial compressive or tensile loads. It was shown that increasing D, L, τ_{max}, $f_c{}'$ of the footing, or the axial compression load, reduce X_{cr}, whereas increasing t, $f_{ct}{}'$ of the CFFT, the fraction of longitudinal fibers in the tube, or the axial tension load, increase X_{cr}. As the axial load eccentricity increases, X_{cr} reduces for tension loads and increases for compression loads, until both cases converge asymptotically to the same X_{cr} value, essentially that at pure bending.

Keywords: connection, footing, CFFT, embedment, model, bond, parametric study.

[1] Postdoctoral Fellow, Department of Civil Engineering, Queen's University, Kingston, ON, K7L 3N6 Canada. E-mail: p.sadeghian@queensu.ca

[2] Professor and Canada Research Chair in Innovative and Retrofitted Structures, Department of Civil Engineering, Queen's University, Kingston, ON, K7L 3N6 Canada. E-mail: fam@civil.queensu.ca

INTRODUCTION

In recent years concrete-filled fiber reinforced polymer (FRP) tubes (CFFTs) have been studied for a variety of structural engineering applications such as bridge piers, piles, and poles (Mirmiran and Shahawy, 1997, and Fam and Rizkalla, 2002). The noncorrosive tube provides protection and confinement for the concrete core, thereby increasing its strength, ductility and durability, in addition to simplifying construction as a stay-in-place form. The laminate structure of the FRP tube can generally be engineered to offer the desired strength and stiffness in a specific direction, by controlling the number of layers and angles at which layers of fibers are oriented. As such, the tube can effectively replace conventional steel reinforcement. Studies have demonstrated several benefits of the concrete fill, including increasing flexural strength and stiffness and preventing local buckling of the tube (Son and Fam, 2008).

The concept of precast CFFTs has been developed by some researchers (Zhu et al., 2004, Qasrawi and Fam, 2008, and Fam, 2008). The combination of precast technology and hybrid construction increase the advantages of CFFT members through rapid construction and quality control. For practical applications, precast CFFTs may be used for poles and piles and are typically subjected to axial and lateral loads. Generally, there are three concepts for connections of CFFT members to reinforced concrete (RC) members: (a) direct embedment; (b) dowel bars; and (c) post-tensioning, however, research in these areas is still very limited.

Direct embedment of CFFTs into RC members greatly simplifies construction, compared to using dowel bars or post-tensioning. Recently, Nelson et al (2008) tested several CFFT cantilevered specimens embedded into RC footings at various embedment lengths, without using dowel bars or post-tensioning. The objective was to establish the critical embedment length X_{cr}, which is the minimum embedment length required to achieve flexural failure outside the footing.

This length was found to be 0.7 times the diameter of the tube used in that particular study. Shorter embedment lengths led to excessive slip and bond failure at lower capacities. Most recently, Sadeghian and Fam (2010) developed a robust analytical model for this type of direct embedment connection of circular CFFTs into RC footings. The model is able to establish X_{cr} required for any combination of bending moment, axial load and shear load. The model was successfully validated using the experimental results.

In this paper, a simplified closed-form analytical expression is developed for X_{cr} under a combination of bending moment, shear load and axial compression load, and verified against the general model (Sadeghian and Fam, 2010). Another model is developed for the case of axial tension load. Also, a comprehensive parametric study is carried out to study the effects of key parameters on X_{cr}. This includes the tube diameter (D), the tube diameter-to-thickness (D/t) ratio, length-to-diameter (L/D) ratio, FRP laminate structure, compressive strength of the CFFT concrete fill ($f_{ct}^{'}$) and footing ($f_{c}^{'}$), bond strength (τ_{max}), and the level and eccentricity of axial compression (P) or tension load (T).

BACKGROUND OF THE ANALYTICAL MODEL

Figure 1(a) illustrates the general layout of a CFFT connection to a concrete footing by direct embedment of a length X, without the use of starter bars or any mechanical connections. The CFFT has an outer diameter D and a length L. The system is subjected to axial and lateral loads P and V. Figure 1(b) shows the free body diagram of the embedded CFFT segment, based on the model by Sadeghian and Fam (2010). The stresses at the CFFT-footing interfaces include transverse radial bearing stresses σ_1 and σ_2 with an inflection point; longitudinal end bearing stress σ_3; and longitudinal bond stress τ. In compression, the bearing stress distributions are

assumed to follow the parabolic stress-strain relationship of concrete, while at the tension interfaces, separation can occur. Bond stresses are applied on the sliding interface in the tension region, following the same linear distribution of slip, which has a zero value at neutral axis and a maximum bond strength τ_{max} at the extreme tension fiber. An analytical formulation for the bond-slip behavior under a slip gradient has been derived from the results of simple push-through tests.

Bearing and bond stresses as well as their resultants F_1, F_2, F_3, and F_4 (Fig. 1(b)), are expressed as functions of five unknown parameters, namely the lengths of bearing interfaces x_1, x_2, and x_3, and the equivalent curvatures α and β from transverse and longitudinal strains. By applying static equilibrium [$\Sigma F_x=0$, $\Sigma F_y=0$, and $\Sigma M=0$] (Fig. 1(b)), three equations are obtained. Two additional equations are derived based on compatibility conditions and the five equations are used to solve for the unknowns. The input parameters are V, P and $M = V.L$, tube outer diameter D, concrete strength f_c' of footing, corresponding strain ε_{co}', concrete Poisson's ratio υ, maximum bond strength τ_{max}, and the corresponding ultimate slip S_u based on push-through tests. The main output of the general model is the embedment length X required to achieve the full bond strength τ_{max}. X_{cr} can then be defined as the minimum X required to achieve failure of the CFFT member outside the footing, simultaneously with a bond failure inside the footing. If $X<X_{cr}$, bond failure occurs before the full potential strength of the CFFT is achieved (i.e. a premature failure).

This model, referred to herein as the 'general model' was used to predict the strength of five cantilever CFFT specimens (C1 to C5) embedded into concrete footings at various embedment lengths and tested in bending, under lateral loading (Nelson et al., 2008). Figure 2 shows the verification of the model using the experimental results, including the predicted X_{cr} of 0.7D. It should be noted that X_{cr} is governed by the capacity of the CFFT member outside the

footing. This capacity, in turn, is governed by the quality of bond between the concrete core and tube which dictates the level of composite action in the CFFT member. In tubes with a smooth inner surface such as those used by Nelson et al (2008), and given the short embedment length, it was difficult to attain an adequate composite action. As such, the concrete core slipped and flexural capacity of the CFFT was limited to that of the tube without the contribution of the concrete core, which represents a lower bound. If the tube has a special treatment such as ridges at the inner surface to develop composite action, the concrete core fully contributes, leading to an upper bound capacity. The predicted X_{cr} based on the lower and upper bound capacities was $0.7D$ and $0.85D$, respectively (Fig. 2). As such, for a conservative design approach, X_{cr} may be established based on the upper bound capacity.

Simplified closed-form expressions for the case of lateral loading only were developed from the general model using some approximations (Fig. 1(c)): (i) it was observed that x_1 and x_2 were very close, therefore can be assumed equal, (ii) x_3/D was very small so F_3 may be applied at the edge of CFFT, and (iii) as bearing stresses were relatively small, they were assumed linear. It is noted that the assumptions were made based on the results of the general model and their justification were provided by Sadeghian and Fam (2010). This led to the expression in Eq. (1) (Fig. 1(c)), referred to herein as 'simplified model (a)':

$$\frac{X}{D} = 5.55 \frac{\tau_{max}}{f'_c} \left(\sqrt{1 + 0.31 \frac{f'_c}{\tau^2_{max}} \frac{M}{D^3}} - 1 \right)$$

(1)

Furthermore, as the couple produced by the longitudinal forces was small compared to that produced by the transverse forces, the F_3 and F_4 forces could be neglected (Fig. 1(d)), leading to Eq. (2), and referred to herein as 'simplified model (b)':

$$\frac{X}{D} = \sqrt{\frac{3\pi M}{D^3 f'_c}}$$

(2)

The assumptions are more logical for the application of the models for some slender cases such as poles. By setting M in these expressions equal to the flexural strength M_u of the CFFT member, X_{cr} can be obtained. The simplified models showed reasonable agreement with the experimental results (Fig. 2). In the following section, a new closed-form model is developed for the general case of loading involving both lateral and axial loads.

A NEW CLOSED-FORM MODEL

In the following sections, closed-form expressions are derived for X_{cr} of CFFT members subjected to eccentric axial compression or tension loads.

Eccentric Axial Compression Load

Figure 3(a) shows the free body diagram of the embedded segment under eccentric axial compression load P and a shear load V. It is assumed that the force F_4 representing bond strength can be neglected, similar to simplified model (b). This assumption is even more logical in this case, because the presence of the external axial compression load P increases the size of the end bearing compression region (x_3 in Fig. 1(b)), while decreasing the tension region where the longitudinal bond strength is generally activated. In addition, the results of the general model showed that the magnitude of forces F_1 and F_2 are much larger than shear load V, thus the effect of V was ignored, in the simplified models. This assumption is even more logical for the application of the models for some high M/V ratios cases. Based on these assumptions, the moment equilibrium equation about point O (Fig. 3(a)) is expressed as follow:

$$P.e = F_1\left(\frac{2}{3}X\right) + F_3(e') \tag{3}$$

where e is the eccentricity of the external load P and e' is the eccentricity of the internal end reaction F_3. Sadeghian and Fam (2010) showed that the force F_1 can be expressed as follows:

$$F_1 = \frac{D \ X \ f_c'}{2\pi} \tag{4}$$

Since F_3 and P are equal when F_4 is neglected, Eq. (3) can be reduced to the following expression:

$$\frac{X}{D} = \sqrt{\frac{3\pi \ P}{D^3 f_c'}(e-e')} \tag{5}$$

The internal eccentricity e' of F_3 is an unknown parameter, which depends on the external eccentricity e. An extreme lower limit would be the external load P applied concentrically (i.e. $e = 0$). In this case, the end bearing stress distribution will be uniform and the resultant reaction F_3 will also be concentric (i.e. $e' = 0$). An extreme upper limit would be the external eccentricity e is infinity (i.e. $P = 0$). In this case, and based on simplified model (a) (Fig. 1(c)), the force F_3 will be applied as a point load at the edge of the CFFT (i.e. $e' = 0.5D$). Equation (6) is proposed to describe the variation of e' with e between the two extreme limits. In this equation, λ is a non-dimensional factor that controls the rate of variation of e' with e. Figure 3(b) is a schematic of the variation of e' with e between the extreme limits as described by Eq. (6) for different values of λ.

$$e' = \frac{D}{2}\left(\frac{e}{e + \lambda D}\right) \tag{6}$$

Equation (5) can then be reduced to the following expression:

$$\frac{X}{D} = \sqrt{\frac{3\pi \ M}{D^3 f_c'}\left(1 - 0.5\left(\frac{e}{D} + \lambda\right)^{-1}\right)} \tag{7}$$

7

The factor λ can be found based on a special condition which is shown schematically in Fig. 3(b). It is hypothesized that if the tension region within the cross-section of the CFFT is reduced to zero (i.e. $x_3 = D$ in Fig. 1(b)), there would be no embedment required for the CFFT member (i.e. $X = 0$), because there is no potential slip. In this case, from Eq. (5), $e' = e$ and the maximum external eccentricity e for a no tension region (i.e. the '*kern*' point) is $D/8$. From Eq. (6) λ will be equal to *3/8*. Equation (7) can then be finalized to the following expression:

$$\frac{X}{D} = \sqrt{\frac{3\pi\, M}{D^3 f_c'}\left(1 - 0.5\left(\frac{e}{D}+\frac{3}{8}\right)^{-1}\right)} \tag{9}$$

In order to check the validity of the $\lambda = 3/8$ value for a wide range of eccentricity e, Eq. (6) has been calibrated in Fig. 3(c), in comparison to the exact e' values established from the general model, for a control parametric case. Generally, reasonable agreement is observed with the $\lambda = 3/8$ simplification, resulting in a slightly higher e'.

Based on this closed-form model which is referred to here as 'simplified model (c)' (Eq.(9)), the embedment length X depends on the CFFT diameter D, concrete strength of footing f_c', external moment M and external eccentricity e. If the external loading is applied as a pure bending (i.e. $P = 0$ and $e = \infty$), Eq. (9) will be reduced to Eq. (2).

The critical embedment length X_{cr}, which is the minimum embedment length required to achieve CFFT failure outside the footing, is related to the axial load-bending moment (P-M) interaction diagram of the CFFT member as shown in Fig. 3(d). Based on this figure, if the load P is applied at an eccentricity e ranging from zero to $D/8$, the critical embedment length X_{cr} will be zero (i.e. the system is theoretically stable without any embedment, though practically speaking, some embedment would be provided). Beyond $e = D/8$, X_{cr} starts increasing, based on the (P-M) interaction curve and also depending on the position of the peak moment point relative

to the pure bending point. If the peak moment point M_p, which may or may not necessarily be the balanced point, is sufficiently higher in value than the pure bending M_o, and as e/D increases, according to Eq. (9) X_{cr} will increase to a peak value, then decreases following an asymptotic curve that approaches X_{cr} corresponding to pure bending. The peak X_{cr} point does not necessarily correspond to the peak moment point M_b, but generally corresponds to a point between M_p and M_o. On the other hand, when the M_p and M_o points on the interaction curve are relatively close, and as e/D increases, X_{cr} curve increases asymptotically, until it approaches X_{cr} of the pure bending condition, without having a peak. This is the most likely scenario, for most practical CFFT member designs, as will be demonstrated in the parametric study.

Eccentric Axial Tension Load

CFFT members may be subjected to an axial tension force due to uplift hydraulic or wind loadings in certain applications such as in marine environments. The general model by Sadeghian and Fam (2010) (Fig. 1(b)) is capable of predicting X_{cr} for the case of CFFT subjected to an axial tension load. The model, however, has a limitation on the eccentricity ($e = M/P$) of the tension force, such that the neutral axis position must be within the cross-section under eccentric tension load (i.e. $x_3 \geq 0$ in Fig. 1(b)). Unlike axial compression loads, it is anticipated that X_{cr} would increase as the eccentricity of the axial tension load reduces. The most critical condition would be a concentric axial tension load applied to an axisymmetric problem. In this case, X_{cr} is the embedment length required to achieve the tensile strength of the CFFT $\left[f_{tu}(\pi D t)\right]$ (governed by FRP tube tensile strength only as the entire concrete core cross-section is fully cracked), simultaneously with bond failure of the CFFT $\left[\tau_{max}(\pi D X_{cr})\right]$ (governed by

bond strength τ_{max} applied uniformly to the embedded surface area). This condition leads Eq. (10) for the case of concentric tensile loading, referred to herein as 'simplified model (d)':

$$\left(\frac{X}{D}\right)_{cr} = \frac{t}{D}\frac{f_{tu}}{\tau_{max}}$$ (10)

PARAMETERIC STUDY

In this section, the simplified models and the general model (Sadeghian and Fam, 2010) are used in a parametric study to investigate the effects of key parameters on the critical embedment length X_{cr}, including: (a) geometric parameters (tube diameter D, thickness t, and length outside footing L), (b) mechanical properties (concrete compressive strength of both the footing (f_c')and CFFT (f_{ct}'), bond strength τ_{max} between the FRP tube and footing, and laminate structure of E-glass/epoxy [0/90]$_s$ cross-ply laminates of the FRP tube, in terms of the ratio of fiber fractions in the longitudinal and hoop directions ($A{:}H$)), and (c) loading conditions (axial load level P in both compression and tension, along with its eccentricity e). While each parameter is being investigated, other parameters are kept constant. The default parametric values are $D = 400$ mm, $f_c' = f_{ct}' = 40$ MPa, $\tau_{max} = 0.75$ MPa, $t = 4$ mm ($D/t = 100$), $L/D = 5$, ($A{:}H$) = (1:2), and $P = 0$.

CFFT Strength under Eccentric Loading outside the Footing

For each case in the parametric study, the objective is to establish X_{cr}, which is controlled by the potential strength of the CFFT member just outside the footing. This strength corresponds to a point on the axial load-bending moment interaction curve, depending on the eccentricity of the applied axial load. If the embedment length $X < X_{cr}$, this potential strength will not be reached, whereas when $X > X_{cr}$, this strength is reached and maintained as a ceiling, regardless of the length X.

Fam and Rizkalla (2002) have developed a model to establish the flexural strength of CFFT members. Later, the model was extended to account for combined bending and axial compression loads (Fam et al. 2003), in order to establish the full interaction curve. The models are based on perfect bond between the concrete core and the FRP tube. They adopt a variable confinement model for the concrete core in compression, which is dependent on the strain gradient of the section (i.e. the eccentricity of the axial load). The variable confinement model makes use of the nonlinear stress-strain function of concrete (Mander et al. 1988). In tension, a tension stiffening effect of concrete is also adopted (Collins and Mitchell 1997). For the FRP tube, a second order function is used to represent the longitudinal stress-strain behavior in both tension and compression as determined by the classical lamination theory (Daniel and Ishai 1994). Failure of the CFFT section is governed by either tension or compression failure of the tube, which leads to establishing the full interaction curve of the section. Since the presence of an axial compression load makes bond failure less critical (i.e. improves conditions), most of the parameters are studied for the case of pure bending first, and then the effects of axial compressive and axial tension loads are studied at the end of the parametric study.

Results of the Parametric Study

Effect of tube diameter: The range of tube diameter D studied was 200 to 600 mm. Figures 4(a) and 4(b) show the variation of bending moment M and normalized moment $M/(D^3 f_c')$ with embedment ratio X/D, respectively, for all cases. Results of the general model and simplified models (a) and (b) are presented in the figures. It is clear that the critical embedment ratio $(X/D)_{cr}$ is dependent on the tube diameter. As D increases, $(X/D)_{cr}$ ratio reduces. For example, increasing the diameter threefold (from 200 to 600 mm) results in reducing $(X/D)_{cr}$ by about 38%. Figure

11

4(a) shows that changing D affects both the flat plateau (i.e. the flexural strength of the CFFT member), as well as the part of the curve governed by bond failure (i.e. the part to the left of $(X/D)_{cr}$). The simplified models (a) and (b) are a little conservative, compared to the general model, as they result in a slightly larger $(X/D)_{cr}$ ratio. Nonetheless they can provide a simple yet reliable tool for design purposes.

Effect of tube thickness: The range of tube thickness t studied was 2.67 to 8.0 mm, which corresponds to diameter-to-thickness D/t ratios of 50 to 150. Figure 5 shows the variation of bending moment M with embedment ratio X/D for all cases. Changing t affects the flat plateau representing flexural strength of the CFFT member, but has no effect on the initial part of the curve representing bond failure. Increasing t increases the moment resistance of CFFT member, and thus increases $(X/D)_{cr}$. For example, increasing t threefold resulted in a 39% increase in $(X/D)_{cr}$. As observed before, simplified models (a) and (b) are slightly conservative but reasonably accurate relative to the general model.

Effect of shear span-to-diameter ratio: The L/D ratios studied are 3, 5, 10, and infinity (i.e. pure bending). Figure 6 shows the variation of bending moment M and the embedment ratio X/D for all cases. It is interesting to note that both simplified models assume that the transverse bearing forces within the embedment length are equal (i.e. both models ignore the shear force at the face of the footing). As such, the L/D parameter can only be studied using the general model. Figure 6 shows that changing the length L for the same diameter D have no effect on the flexural strength of the CFFT member (i.e. the flat plateau); however, it affects the initial part of the curve governed by bond failure. This is because the change in the shear forces V, resulting from

the change of *L*, causes some change in the balance of the internal forces within the embedment length. As *L/D* ratio is reduced, $(X/D)_{cr}$ is increased, however, the effect appears to be very small. Both simplified models, especially model (b), seem to agree reasonably well with the general model, despite the fact that they ignore the CFFT length effect and hence the shear force.

Effect of concrete compressive strengths of CFFT and footing: The range of concrete strength f_{ct}' (i.e. for CFFT) and f_c' (i.e. for footing) studied was 20 to 60 MPa. Figures 7(a) and 7(b) show the variation of the bending moment *M* and the normalized moment $M/(D^3 f_c')$ with the embedment ratio *X/D*, respectively. For a given constant f_c' of the footing, changing f_{ct}' of the CFFT affects its flexural strength (i.e. the flat plateau) but does not influence the initial part of the curve, which is governed by bond failure. In this case, the critical embedment ratio $(X/D)_{cr}$ is increased as f_{ct}' of the CFFT member increases. On the other, for a given constant f_{ct}' of the CFFT, changing f_c' of the footing has no effect on the CFFT flexural strength (i.e. the flat plateau) but significantly affects the initial part of the curve, governed by bond failure. In this case, the critical embedment ratio $(X/D)_{cr}$ is reduced as f_c' of the footing increases. If concrete strength is the same for the CFFT member and footing (i.e. $f_c' = f_{ct}'$), and is changed in both elements simultaneously, then $(X/D)_{cr}$ will also be reduced but at a lesser rate as f_c' increases. For example, increasing f_c' threefold (from 20 to 60 MPa) helps reducing $(X/D)_{cr}$ by 28% only. The figures also show that the results of simplified model (a) are much closer to the general model than simplified model (b) and the simplified models are generally conservative.

Effect of bond strength between FRP tube and footing: The range of bond strength τ_{max} studied was 0 to 2 MPa. In the FRP tubes tested by Nelson at al (2008), the measured bond

strength was 0.71 MPa. In this study, the selected range is intended to cover perhaps a variety of surface textures of FRP tubes. Zero bond strength reflects a worst case scenario of a tube surface that may be contaminated and subsequently debonded from concrete. Figure 8 shows the variation of bending moment M with embedment ratio X/D for all cases. The change in τ_{max} affects the initial part of the curve governed by bond failure, but has no effect on the flat plateau representing flexural strength of the CFFT member. The figure shows that the critical embedment ratio $(X/D)_{cr}$ is reduced as τ_{max} increases. For example, increasing τ_{max} from 0 to 2 MPa results in reducing $(X/D)_{cr}$ by 22%. It is worth noting that simplified model (b) neglects the longitudinal internal forces, including the bond stress resultant. As such, only one prediction is given by simplified model (b) for all cases of τ_{max} in Fig. 8, since τ_{max} is not a parameter in Eq. 2. This indicates that the accuracy of simplified model (b) is not dependent on τ_{max}. For $\tau_{max}= 0$, it varies from the general model by as much as 26% for $(X/D)_{cr}$, while simplified model (a) agrees reasonably well with the general model.

It should be noted that the bond strength between the outer face of FRP tubes and concrete footing is a function of concrete strength, roughness of the tube surface, and normal stress on the surface. This subject is complicated and more research is needed. Thus in this research, the effects of bond strength and concrete strength have been studied separately.

Effect of FRP tube laminate structure: The range of E-glass/epoxy GFRP tube cross-ply $[0/90]_s$ symmetric laminates studied was $(1_{(A)}:3_{(H)})$ to $(3_{(A)}:1_{(H)})$. For example, $(1_{(A)}:3_{(H)})$ means that one quarter part of fibers are oriented in axial direction of tube and three quarter parts of fibers in hoop direction. Figure 9(a) shows the longitudinal stress-strain curves of the tubes in tension and compression as predicted by the classic lamination theory (Daniel and Ishai, 1994).

Figure 9(b) shows the effect of the laminate structures on the embedment length. Similar to the

tube thickness t, laminate structure affects the flexural strength of the CFFT member (i.e. the flat

plateau) but has no effect on the initial part of the curve governed by bond failure. As the

fraction of longitudinal fibers increase, the moment capacity also increases, and as a result,

$(X/D)_{cr}$ also increases. Once again, the simplified models are conservative but acceptable.

Effect of axial compression load: In order to consider the effect of axial compression load

and bending moment on the embedment length, a wide range of eccentricity ratio e/D (zero,

representing pure axial load, to infinity, representing pure bending) was studied. In addition, for

better understanding of the effect of this parameter, various GFRP tubes (with D/t ranging from

50 to 150) were studied under the combined effects of axial load and bending moment. As

indicated earlier, X_{cr} depends on the (P-M) interaction curve of the CFFT member. Figure 10

shows the (P-M) curves for the selected CFFT members. The curves were established using the

variable confinement model developed by Fam et al. (2003) for the eccentric axial compression

range (i.e. the +ve e/Ds). The interaction curves for the eccentric axial tension load range (i.e. the

-ve e/D) are also shown in Fig. 10 and were also established using the Fam et al. (2003) model,

but ignoring concrete confinement (i.e. using a concrete model similar to that used to establish

the pure bending point). An average laminate structure of ($I_{(A)}:I_{(H)}$) was selected, because both

longitudinal and hoop fibers are important for the (P-M) curves. It is worth noting that the

interaction curves on the compression load side were governed by compression failure within the

entire range of e/D, even for the pure bending point, for all D/t ratios, except for the $D/t = 150$

curve. What appears as 'belly' in these curves, with a moment slightly higher than the pure

bending point is, in fact, not a balanced point, as was also observed by Fam et al (2003). This is a

result of the unique nature of the stress-strain curves of the FRP tubes, where the tensile strength is considerably higher than the compressive strength (Fig. 9(a)). Therefore, the interaction curves on the tension load side for these specific cases show distinct kinks representing real balanced points when failure changes from the compression to the tension side.

Figure 11 shows the variation of critical embedment ratio $(X/D)_{cr}$ with the eccentricity ratio e/D for the various tubes, based on the general model and simplified model (c). The figure shows that up to $e/D = 1/8$, no tension is developed and in theory end bearing is sufficient (i.e. $(X/D)_{cr} = 0$). Beyond this point, as e/D increases, $(X/D)_{cr}$ also increases very rapidly up to e/D of about 0.75, and then gradually stabilizes, approaching a value equivalent to that of pure bending (i.e. at $e/D = \infty$). It can be concluded that the presence and increase of an axial compression load reduces the necessary embedment length. It is noted that the set of curves in Fig. 11 are similar to the lowermost curve in Fig. 3(d) (i.e. do not have a peak higher than the asymptote). This is because the pure moment and peak moment points on the (P-M) interaction curves are relatively close. Figure 11 also shows that simplified model (c) is somewhat conservative in that it overestimates $(X/D)_{cr}$ by about 16 to 19%, relative to the general model. Nonetheless, it should be quite reliable for design purposes.

Effect of axial tension load: The worst case scenario under axial tension load is when it is concentric ($e/D = 0$). Figure 12 shows the effect of τ_{max} on $(X/D)_{cr}$ for different FRP tube laminate structures, according to simplified model (d) (Eq. 10). The figure shows that, as τ_{max} increases, $(X/D)_{cr}$ is significantly reduced, whereas when the tensile strength of the FRP tube increases (i.e. by increasing the fraction of longitudinal fibers), $(X/D)_{cr}$ also increases.

In order to study the effect of e/D of the axial tension load on $(X/D)_{cr}$, the (P-M) interaction curves have been established (Fig. 10). Figure 13 shows the variation of $(X/D)_{cr}$ with e/D of the axial tension load for the CFFTs with two extreme D/t ratios of 50 and 150. Also shown for reference are the variations for the axial compression load cases. It is clear that, unlike eccentric compression loads, as e/D reduces, $(X/D)_{cr}$ increases for the eccentric tension load. On the other hand, as e/D increases, $(X/D)_{cr}$ for both cases of axial tension and compression loads converge to a similar value, essentially that at pure bending. It also appears that at a given eccentricity e/D, the effect of D/t on $(X/D)_{cr}$ is much higher in tension than in compression.

CONCLUSIONS

In this paper new closed-form models have been developed to establish the critical embedment length X_{cr} of concrete-filled FRP tubes (CFFTs) fixed into concrete footings. The CFFTs may be subjected to a general case of loading comprising lateral and axial compression or tension loads. The models enable designers to establish the specific X_{cr} necessary to develop the full strength of the CFFT member at any point on its axial load-bending moment interaction curve. The simplified closed-form models, along with the general model by Sadeghian and Fam (2010), were used in a comprehensive parametric study. The following conclusions are drawn:

1. With regard to geometric properties, it was shown that increasing the CFFT diameter, or the CFFT length out side the footing, reduces X_{cr}, whereas increasing the CFFT tube thickness increases X_{cr}.

2. With regard to mechanical properties, it was shown that increasing bond strength between the FRP tube and concrete footing, or the concrete compressive strength of the footing, reduces X_{cr}. On the other hand, increasing the concrete compressive strength inside the FRP tube, or

17

increasing the longitudinal strength of the tube by increasing the proportion of fibers in the longitudinal direction, increases X_{cr}.

3. With regard to loading conditions, it was shown that increasing the axial compression load, or reducing the eccentricity, reduces X_{cr}. In fact, at eccentricities lower than 1/8 of the diameter, the CFFTs in theory do not need any embedment (i.e. $X_{cr} = 0$). On the other hand, for axial tension loads, as the eccentricity is reduced, X_{cr} is increased until its maximum value is reached at zero eccentricity. As the eccentricity increases, X_{cr} reduces for tension loads and increases for compression loads until both cases converge to the same asymptotic value corresponding to pure bending.

ACKNOWLEDGEMENTS

NOTATION

D	=	tube outer diameter;
e	=	eccentricity of external load P;
e'	=	eccentricity of internal end reaction F_3;
F_i	=	resultant force on interface i;
f_c'	=	concrete strength of footing;
f_{ct}'	=	concrete strength of CFFT;
i	=	code of interface (1, 2, 3, or 4);
L	=	length of CFFT at the outside of footing;

M	=	bending moment;
M_o	=	resistance pure bending moment of CFFT;
M_p	=	peak resistance bending moment of CFFT in interaction curve;
M_u	=	resistance bending moment of CFFT;
P	=	compressive axial load;
S_u	=	ultimate slip;
T	=	tensile axial load;
t	=	tube wall thickness;
V	=	shear load;
X	=	embedment length;
X_{cr}	=	critical embedment length;
x_i	=	bearing length of interface i;
α	=	equivalent curvatures of transverse strains;
β	=	equivalent curvatures of longitudinal strains;
λ	=	non dimensional factor of internal eccentricity;
ε_{co}'	=	concrete strength corresponding strain;
υ	=	concrete Poisson's ratio;
σ_i	=	bearing stress on interface i;
τ	=	bond stress; and
τ_{max}	=	bond strength.

REFERENCES

1. Collins, M. P., and Mitchell, D. (1997). Prestressed concrete structures, Response Publications, Canada.

2. Daniel, I. M., and Ishai, O. (1994). Engineering mechanics of composite materials, Oxford University Press, New York.

3. Fam, A. (2008). "Development of a novel pole using spun-cast concrete into FRP tubes." *PCI Journal*, 53(3), 100–113.

4. Fam, A. Z., and Rizkalla, S. H. (2002). "Flexural behavior of concrete-filled fiber-reinforced polymer circular tubes." *ASCE Journal of Composites for Construction*, 6(2), 123–132.

5. Fam, A., Flisak, B., and Rizkalla S. (2003). "Experimental and analytical modeling of concrete-filled fiber-reinforced polymer tubes subjected to combined bending and axial loads." *ACI Structural Journal*, 100(4), 499–509.

6. Mander, J. B., Priestley, M. J. N., and Park, R. (1988). "Theoretical stress-strain model for confined concrete." *ASCE Journal of Structural Engineering*, 114(8), 1804–1826.

7. Mirmiran, A., and Shahawy, M. (1997). "Behavior of concrete columns confined by fiber composites." *ASCE Journal of Structural Engineering*, 123(5), 583–590.

8. Nelson, M., Lai, Y. C., and Fam, A. (2008). "Moment connection of concrete-filled fiber reinforced polymer tubes by direct embedment into footings." *Advances in Structural Engineering*, 11(5), 537–547.

9. Qasrawi, Y., and Fam, A. (2008). "Flexural load tests on new spun-cast concrete-filled fiber-reinforced polymer tubular poles." *ACI Structural Journal*, 105(6), 750–759.

10. Sadeghian, P., and Fam, A. (2010). "Bond-slip analytical formulation towards optimal embedment of concrete-filled circular FRP tubes into concrete footings." *ASCE Journal of Engineering Mechanics*, 136(4), 524–533.

11. Son, J., and Fam, A. (2008). "Finite element modeling of hollow and concrete-filled fiber composite tubes in flexure: model development, verification and investigation of tube parameters." *Engineering Structures*, 30(10), 2656–2666.

12. Zhu, Z., Mirmiran, A., and Shahawy, M. (2004). "Stay-in-place fiber reinforced polymer forms for precast modular bridge pier system." *ASCE Journal of Composites for Construction*, 8(6), 560–568.

List of Figures:

(a) Geometry of the problem
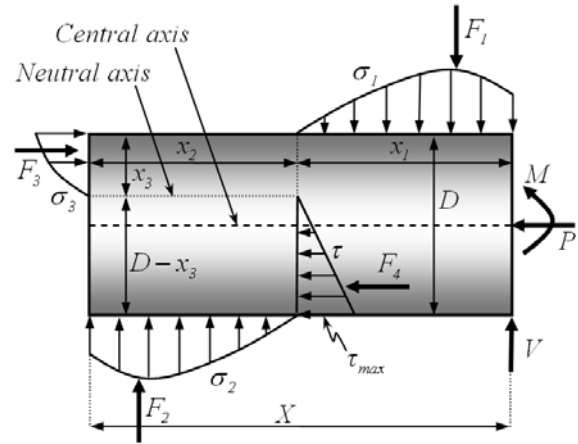
(b) General model
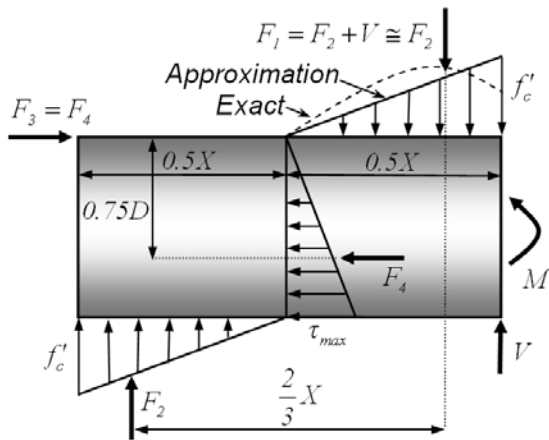
(c) Simplified model (a)
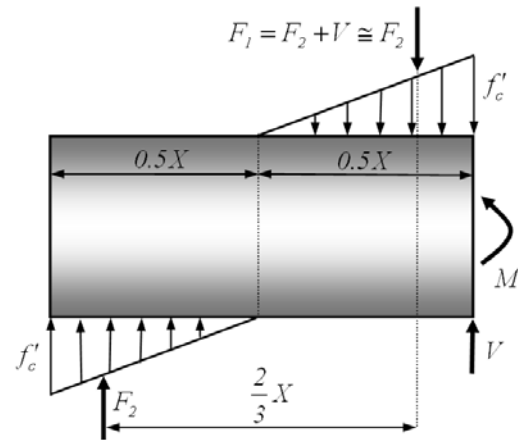
(d) Simplified model (b)

Fig. 1. Free body diagrams of the general and simplified models
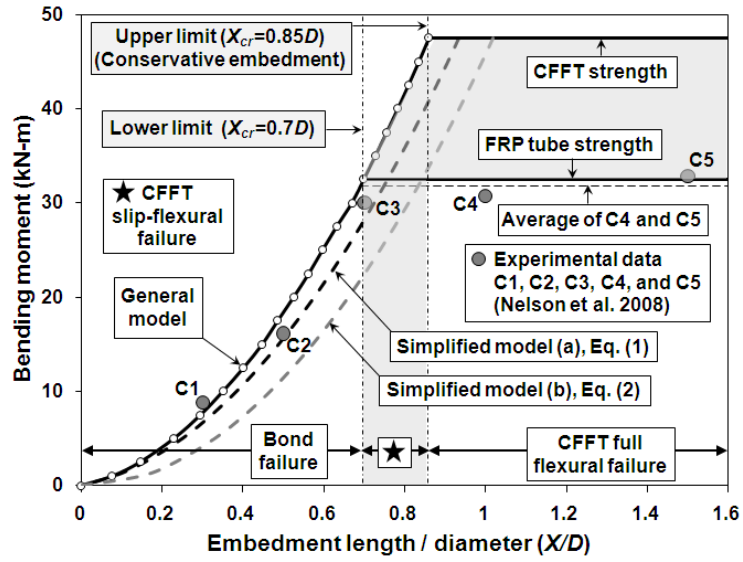
Fig. 2. Verification of the general and simplified models
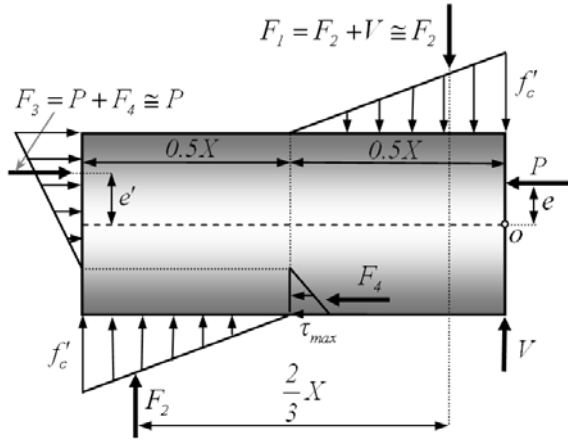
(a) Simplified model (c)
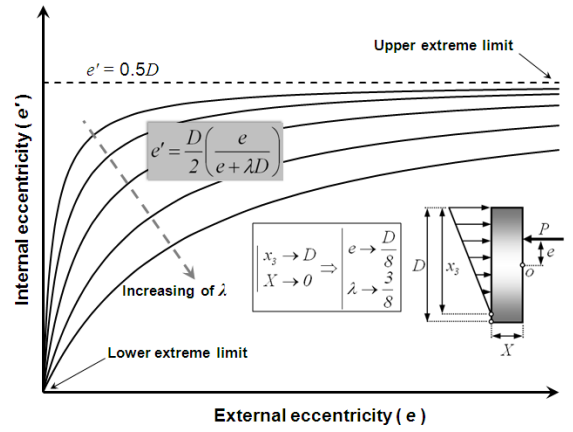
(b) Proposed equation for internal eccentricity e'
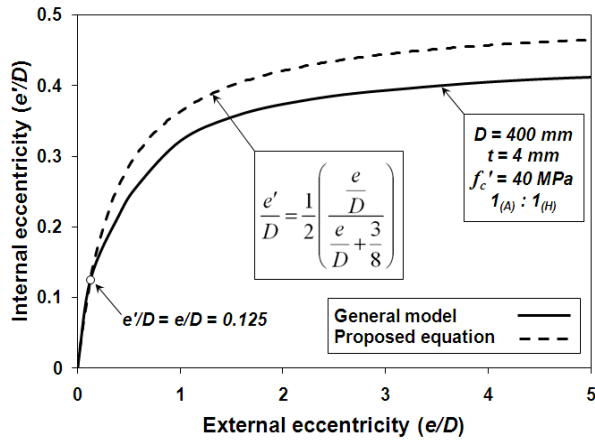
(c) Calibration of expression for e'
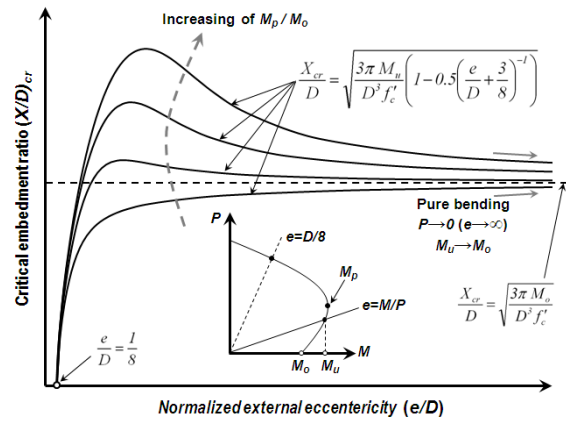
(d) Effect of e on X_{cr}

Fig. 3. Mechanics and performance of new closed-form simplified model (c)
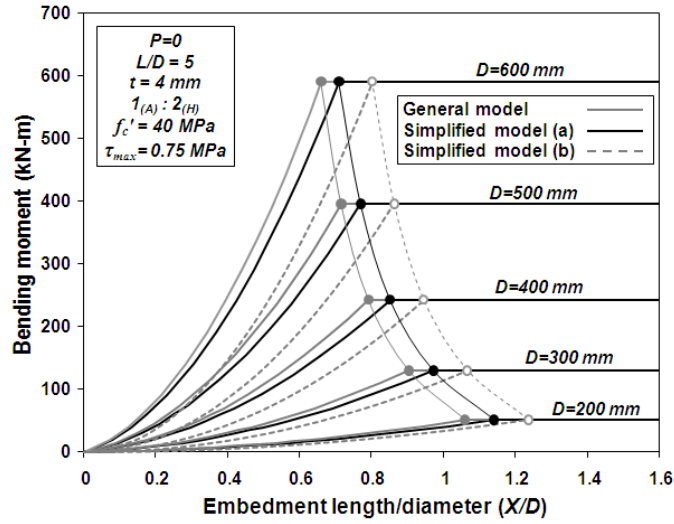
(a) Variation of moment with *X/D*
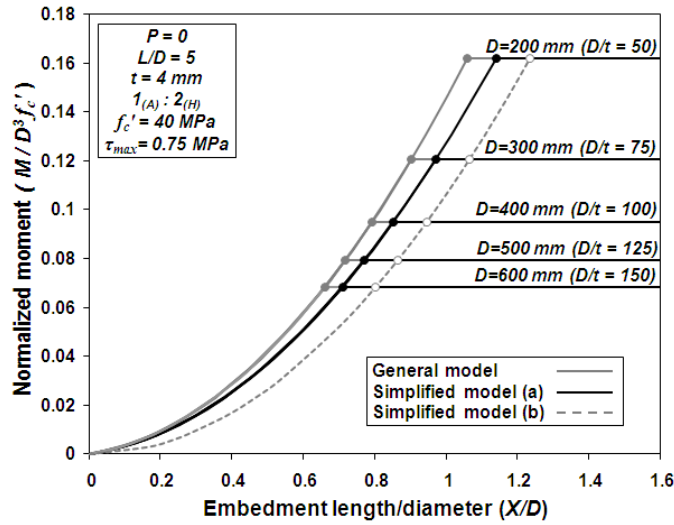
(b) Variation of normalized moment with *X/D*

**Fig. 4. Effect of tube diameter on critical embedment depth**
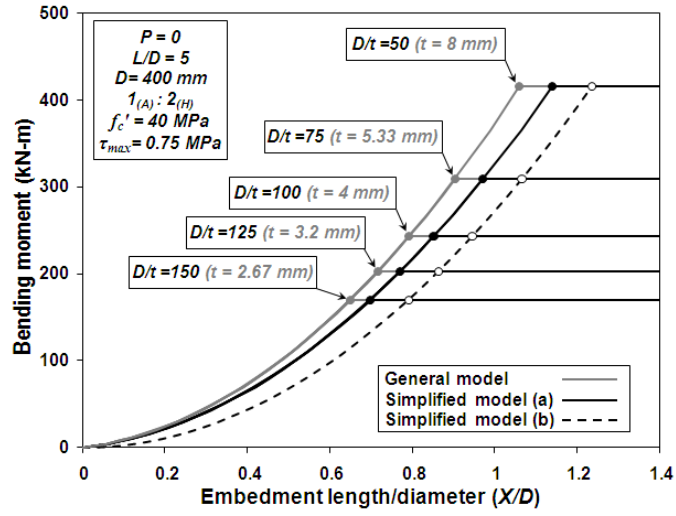
Fig. 5. Effect of tube thickness on critical embedment depth
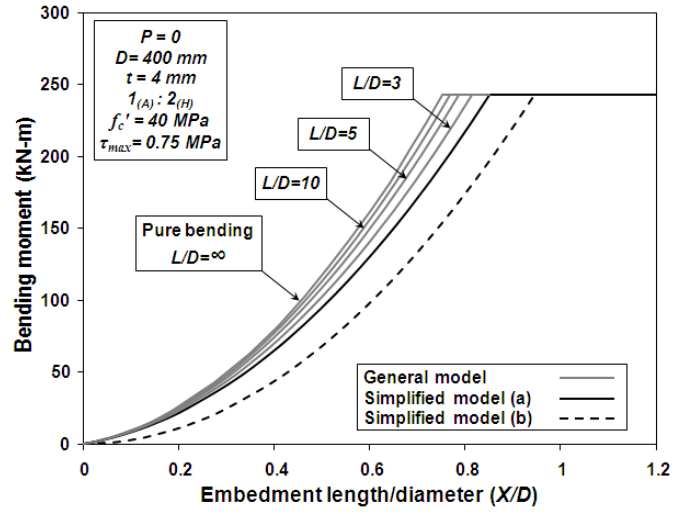
Fig. 6. Effect of shear span ratio on critical embedment depth
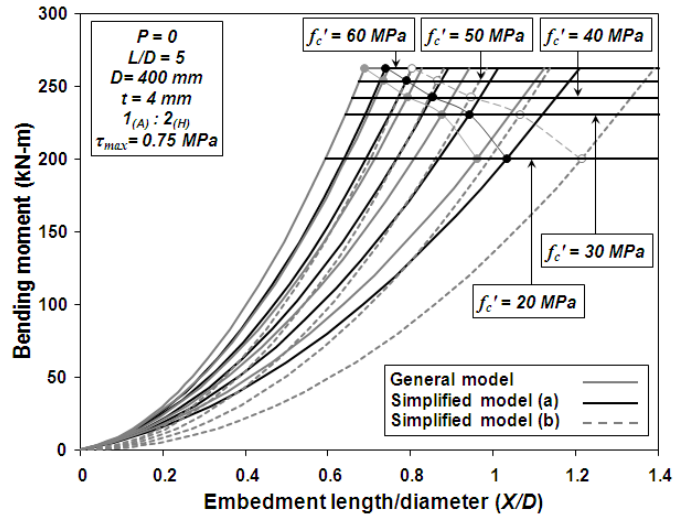
(a) Variation of moment with *X/D*
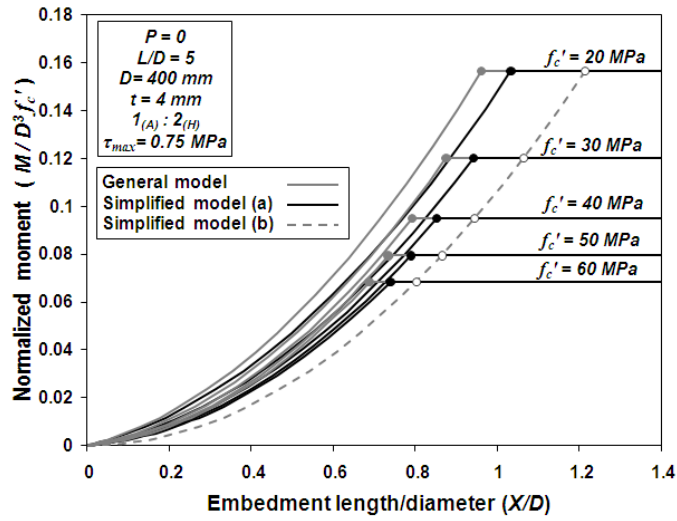
(b) Variation of normalized moment with *X/D*

Fig. 7. Effect of concrete strength on critical embedment depth
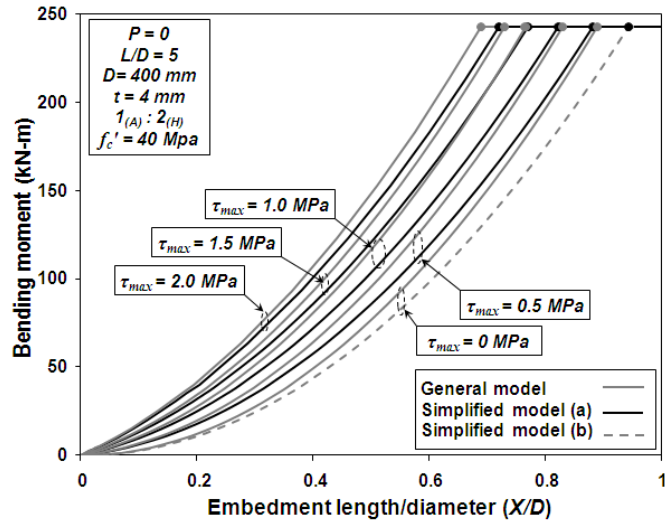
Fig. 8. Effect of bond strength on critical embedment depth
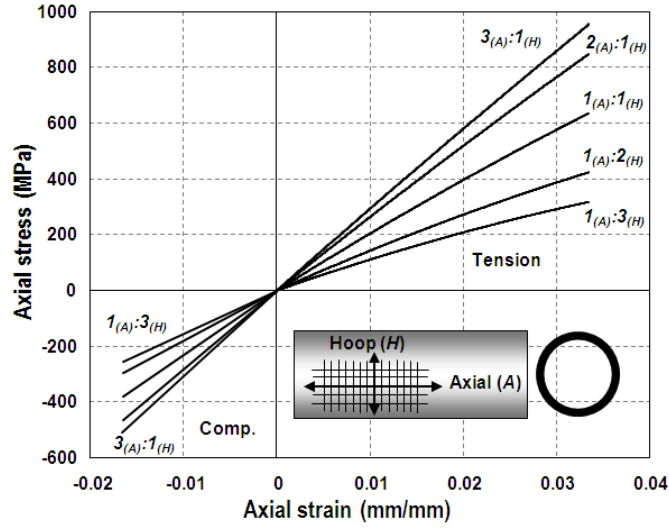
(a) Stress-strain curves of [0/90]ₛ GFRP tubes in axial direction
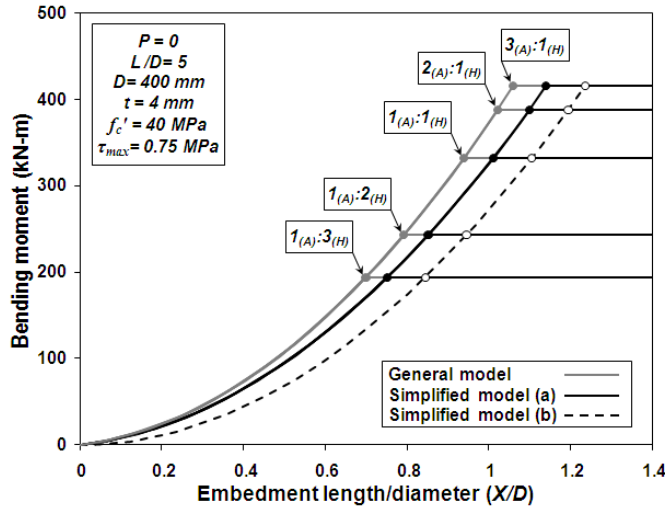
(b) Variation of moment with embedment length

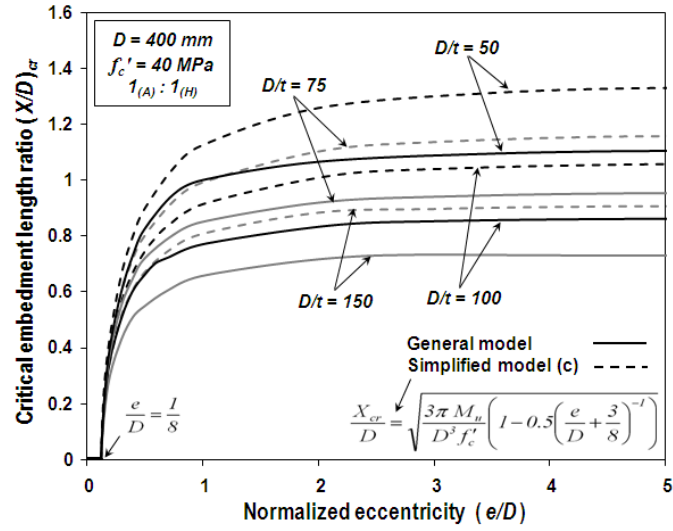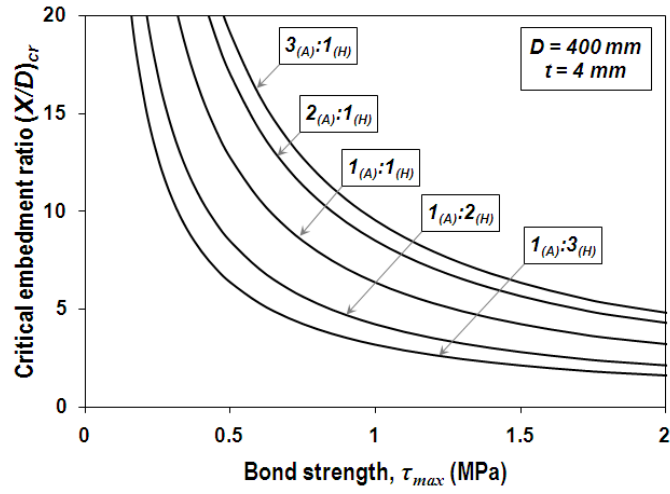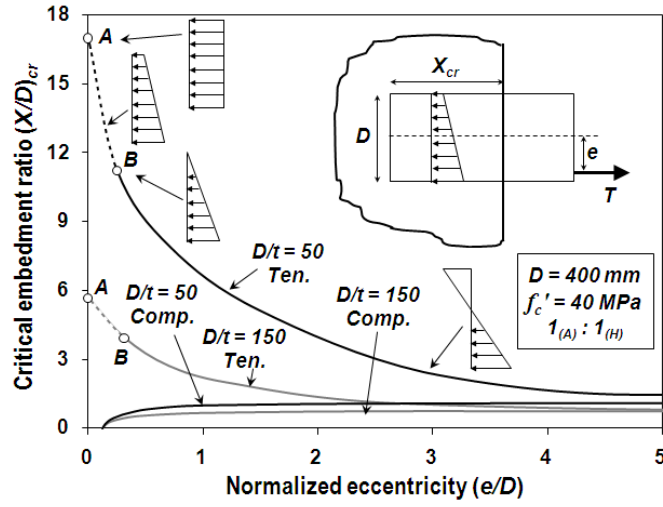**Fig. 9. Effect of laminate structure on critical embedment depth**
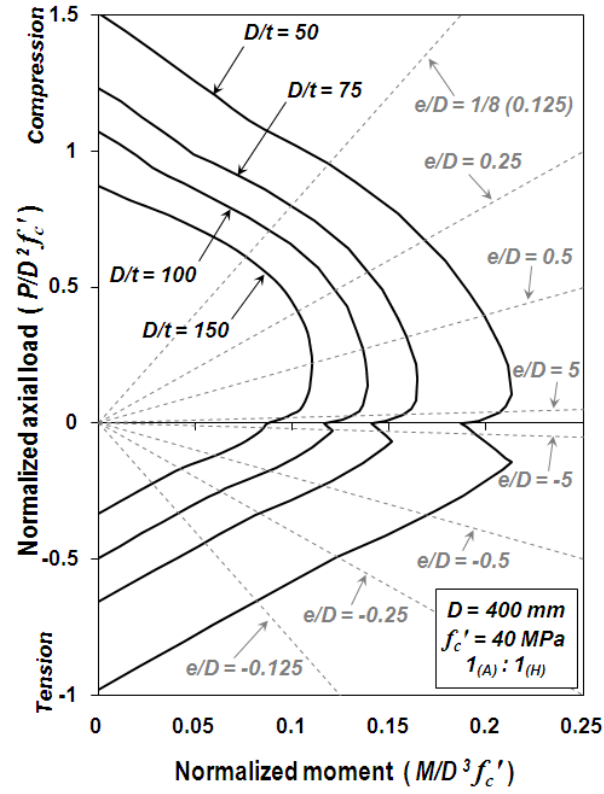
Fig. 10. Normalized axial load-moment interaction curves of CFFTs

Fig. 11. Effect of eccentric compressive load on critical embedment depth

Fig. 12. Effect of bond strength on critical embedment under concentric tensile load

Fig. 13. Effect of eccentric tensile load on critical embedment depth

13